UNIVERSITY OF TURKU

Ignition delay and laminar flame speed calculations of hydrogen/oxygen/argon and methane/oxygen/argon mixtures

Department of Mechanical and Materials Engineering

Bachelor's thesis

Author:
Rasmus Tomma

27.4.2026
Turku

Bachelor's thesis

Subject: Mechanical Engineering

Author(s): Rasmus Tomma

Title: Ignition delay and laminar flame speed calculations of hydrogen/oxygen/argon and methane/oxygen/argon mixtures

Supervisor(s): D.Sc. Armin Wehrfritz

Number of pages: 41 pages

Date: 27.4.2026

To adhere to global climate agreements and avoid climate change, alternative emission-free power generation technologies must be found. The Argon Power Cycle is one of the promising future solutions. It offers great efficiency with low emissions since it uses argon as a working fluid instead of nitrogen, which generates toxic nitrogen oxide (NO_x) emissions. This technology also makes post-combustion carbon capture feasible. With this promising performance, new challenges are also introduced, such as combustion instability and engine knock.

The aim of this Bachelor's thesis is to evaluate the combustion characteristics of hydrogen/oxygen/argon and methane/oxygen/argon mixtures by simulating their behavior with a Python script utilizing the Cantera kinetics library in combination with the AramcoMech 3.0 kinetic model. The two parameters studied are ignition delay time (IDT) and laminar flame speed (S_L). The simulations were conducted under varying thermodynamic conditions across a temperature range of 900–1600 K, a pressure range of 1–100 bar, and an equivalence ratio of 0.5–2.0.

The simulations reveal hydrogen's ideal behavior in an argon atmosphere by accelerating the combustion, thus shortening the ignition delay time and increasing the laminar flame speed compared to the air-diluted benchmarks. This is achieved due to argon's higher specific heat ratio. Methane exhibited more complex behavior in the argon atmosphere. The laminar flame speed almost doubled compared to the air-diluted benchmark, but the ignition delay suffered at high pressures. This is caused by the extreme dilution required to keep the combustion stable for the less reactive methane, thus outweighing argon's thermodynamic benefits.

The Argon Power Cycle offers promising results for the future, but still requires more optimization and research. Reactive fuels such as hydrogen work well with this technology, but less reactive fuels such as methane require precise balancing of dilution and combustion stability. These findings serve as a foundation for more sophisticated 3D modeling and validation by experiments.

Kansainvälisten ilmastosopimusten noudattaminen ja ilmastonmuutoksen torjuminen edellyttävät vaihtoehtoisten, päästöttömien energiantuotantoteknologioiden löytämistä. Aargon-voimakierto on yksi lupaavista tulevaisuuden ratkaisuista. Se tarjoaa erinomaisen hyötysuhteen ja alhaiset päästöt, sillä se käyttää työaineena argonia typen sijaan, joka aiheuttaa myrkyllisiä typpioksidipäästöjä (NO_x). Tämä teknologia tekee myös palamisen jälkeisestä hiilidioksidin talteenotosta toteuttamiskelpoista. Tämän lupaavan suorituskyvyn myötä syntyy kuitenkin myös uusia haasteita, kuten palamisen epävakautta ja moottorin nakutusta.

Tämän kandidaatintutkielman tavoitteena on arvioida vety/happi/argon- ja metaani/happi/argon-seosten palamisominaisuuksia simuloimalla niiden käyttäytymistä Python-koodilla, joka hyödyntää Cantera-kinetiikkakirjastoa yhdessä AramcoMech 3.0 -kinetiikkamallin kanssa. Tutkittavat parametrit ovat syttymisviive (IDT) ja laminaarinen liekin nopeus (S_L). Simulaatiot suoritettiin vaihtelevissa termodynaamisissa olosuhteissa lämpötila-alueella 900–1600 K, 1–100 barin painealueella sekä seossuhteella 0,5–2,0.

Simulaatiot osoittavat vedyn ihanteellisen käyttäytymisen argon seoksessa, joka kiihdyttää palamista lyhentäen siten syttymisviivettä ja kasvattaen laminaarista liekki nopeutta verrattuna ilmalla laimennettuihin vertailuarvoihin. Tämä johtuu argonin korkeammasta ominaislämpökapasiteettien suhteesta. Metaani käyttäytyi argon seoksessa monimutkaisemmin. Laminaarinen liekki nopeus lähes kaksinkertaistui ilmalla laimennettuun vertailuarvoon nähden, mutta syttymisviive heikkeni korkeissa paineissa. Tämä johtuu voimakkaasta laimennuksesta, jota vaaditaan pitämään palaminen vakaana vähemmän reaktiiviselle metaanille, mikä lopulta kumoaa argonin termodynaamiset edut.

Argon-voimakierto tarjoaa lupaavia tuloksia tulevaisuutta ajatellen, mutta vaatii vielä lisää optimointia ja tutkimusta. Reaktiiviset polttoaineet, kuten vety, toimivat hyvin tämän teknologian kanssa, mutta vähemmän reaktiiviset polttoaineet, kuten metaani, vaativat tarkkaa tasapainottamista laimennuksen ja palamisen vakauden välillä. Nämä tulokset toimivat perustana edistyneemmälle 3D-mallinnukselle ja kokeelliselle validoinnille.

Keywords: Argon Power Cycle, combustion kinetics, ignition delay time, laminar flame speed, Cantera, AramcoMech 3.0, hydrogen, methane, argon.

Table of contents

1 Introduction

1.1 Background

The excessive accumulation of greenhouse gas emissions in the atmosphere represents one of the most critical challenges of our time. In response to global climate change, numerous nations have committed to achieving carbon neutrality by 2050 [1,2]. This imperative forces the energy and heavy transport sectors to rapidly evolve to meet these stringent targets. Even though they are not the most environmentally friendly, most of the world's infrastructure still heavily relies on internal combustion engines (ICEs) and gas turbines. In order to move away from these technologies or make them more environmentally friendly, rigorous research is required.

The previously mentioned sectors, for the most part, still rely on traditional air-breathing combustion technology. The ambient air, which these engines use, consists of 21% oxygen (O_2) and 79% nitrogen (N_2) by volume. As is known, burning hydrocarbon fuels produces a lot of carbon dioxide (CO_2) emissions, but in addition to these problematic emissions, the high peak operating temperatures in the engine cause nitrogen oxides (NO_x) to form by the oxidation of nitrogen. In addition, NO_x can also form as a result of nitrogen in the fuel and via the prompt NO pathway, and it is an extremely toxic pollutant [3]. Since traditional engine concepts draw in a lot of unnecessary nitrogen, the exhaust stream is also highly diluted by it, making post-combustion carbon capture of the CO_2 quite expensive and hard to achieve. In light of these problems, it is vital to eliminate these emission sources in order to adhere to global climate targets [4].

As mentioned, the traditional engine concept has its downfalls and restrictions. To generate energy and keep heavy transportation moving, new novel closed-loop engine concepts have been developed to overcome these restrictions. These concepts include, for example, the Allam cycle that uses CO_2 as the working fluid, the Graz cycle that uses water as the working fluid, and of course, the Argon Power Cycle (APC) that this study focuses on [5]. Unlike in traditional engines, in the Argon Power Cycle, the ambient air consisting of nitrogen and oxygen has been replaced with pure argon and oxygen [6]. In this way, the nitrogen can be removed from the combustion, thus completely erasing the formation of nitrous oxides. As an added benefit from removing the nitrogen, the

exhaust stream is not overly diluted by it, thus making the separation of water from the exhaust gas by condensation possible, leaving only argon and CO_2 in the stream where they can be separated as well. This makes post-combustion carbon capture feasible and economically viable when using hydrocarbon fuels like methane. When hydrogen is used as the fuel, the carbon emissions can be reduzed almost to zero, leaving the only emission source as the lubrication oil burned during the combustion. In addition to achieving really low emissions, Argon Power Cycle can also achieve notably high efficiency due to higher specific heat ratio (γ) posessed by argon. This increased efficiency caused by the high specific heat ratio is the primary benefit of the Argon Power Cycle [7].

The primary goal of this thesis is to calculate two critical combustion parameters, ignition delay time and laminar flame speed. The simulation results are also compared against traditional air-diluted benchmarks. Simulating these processes is vital, as the use of argon fundamentally alters combustion kinetics and introduces challenges such as engine knock and combustion instability [8]. To model these kinetics, Python scripts utilizing the Cantera kinetics library [9] are utilized.

For grammar checking and language refining purposes an Ai software, Google Gemini was used during the writing of the thesis. The software was also used to troubleshoot coding syntax errors.

1.2 Ignition delay

Regarding the modeling of engine cycles and combustion characteristics, ignition delay is one of the two most critical parameters, alongside laminar flame speed [7,10]. The importance of ignition delay comes from its significant influence on thermal efficiency, pollutant emissions and engine noise [7].

Ignition delay is defined as the time period from a set temperature and pressure of a combustible gas mixture to the onset of ignition [11]. In the context of compression ignition engines, ignition delay is defined as the time interval between the start of fuel injection and the start of combustion [10]. In engine research, ignition delay is usually characterized using the pressure-crank angle (p-θ) diagram, defining the delay as the

crank angle interval between the start of injection and the onset of combustion, with the crank angle serving as a measure of time [10].

When analyzing ignition delay mechanisms, the total delay is divided into chemical and physical factors. In compression ignition processes, such as those utilized in the Argon Power Cycle, the total ignition delay is considered the sum of these two contributions. The chemical factor of the delay stems from the complex chemical reaction paths, beginning from the reactants and ending in the reaction products [12]. The complexity of the reaction paths and species becomes clear when, for example, reviewing the Aramco-II-2016 mechanism which consists of thousands of reactions and hundreds of species for methane combustion [13]. Even the shortened mechanism for the ease of calculations including only species with two or less carbon atoms contains 490 reactions and 86 species [13].

In this thesis, the focus is on the chemical kinetics as the simulation tool Cantera [9] primarily models the chemical ignition delay by assuming the mixture to be homogeneous and pre-mixed. Using the constant volume batch reactor (0D) found in Cantera [9] leaves the physical phenomena out of the calculation. In practical engine applications, the physical factors such as mixing, turbulence and heat losses, would increase the total ignition delay compared to the idealized simulations [7].

1.3 Laminar flame speed

Parallel to ignition delay, the laminar flame speed (S_L) serves as a fundamental indicator of combustion behavior when it comes to modeling the engine performance [7,14]. Laminar flame speed is closely tied to the stability of the engine and the combustion cycle, thus being a vital element of the engine performance [7].

The laminar flame speed is defined as the velocity of a free adiabatic flame propagating towards unburned reactants. It is a physicochemical property of the mixture and is usually modeled as a one-dimensional phenomenon [14,15].

To avoid the computational intensity of Computational Fluid Dynamics (CFD) simulations, certain simplifications and assumptions must be made; these simplifications are also applied in this thesis when modeling the flame speeds. The

flame is assumed to be unstretched, premixed and non-turbulent. Although in real combustion engines the conditions are typically turbulent, the laminar flame speed remains a fundamental requirement for predicting the turbulent flame speeds [16].

Although these simplifications are made to make the use of Cantera possible, the software is capable of accounting for several critical physical phenomena. To calculate the laminar flame speeds Cantera's Free Flame solver (1D) is used. Unlike the zero-dimensional ignition delay models, this solver considers transport properties, fluid flow and molecular diffusion processes. This allows for a more broad analysis of how the chemical and physical transport mechanisms interact during the combustion [9].

1.4 Experimental validation framework

Numerical simulations typically cannot fully replicate real-world phenomena due to their inherent complexity; therefore, certain assumptions and simplifications must be made to make the modeling computationally feasible. As stated by Heywood [7], modeling engine processes involves an appropriate number of assumptions and simplifications that permit the analysis of the critical features. The results acquired by simulations must be critically reviewed and compared with results derived from experiments made in real-world scenarios.

High-fidelity simulations capable of precise quantitative results have been established and are nowadays quite widely used in the industry but due to their extreme computing power requirements, these models tend to be considerably costly [7,17]. Although simpler numerical computational approaches with some assumptions tend to give less accurate results compared to these high-end quantitative simulations, they are often preferred due to their lower costs, especially at the start of the research. It should be noted that these simplified simulations can yield good approximations that can be critically used to derive conclusions regarding the observed phenomena [17].

In the following subsections, these experimental methods and correlations are discussed, and a benchmark for comparing the simulations to existing empirical data is

established. This comparison provides the necessary context for the conclusions drawn later in this thesis.

1.4.1 Ignition delay

In order to enable the use of different convenient calculation and simulation tools such as Cantera, a lot of experimental data must be collected. The reliability of such tools is fundamentally related to the availability of high-quality empirical data.

Often ignition delay experiments are conducted as shock tube experiments, since it is an extensively researched method that has been characterized in fine detail. Piezoelectric pressure transducers are used in conjunction with time interval counters to measure shock velocities, while a photomultiplier is used to track the hydroxyl radical (OH*) chemiluminescence. The ignition delay can then be derived as the time interval between the linear extrapolation of the steepest increase of OH* emission signal compared to the baseline and the arrival of end-wall reflected shock waves [8,18–20].

Ultimately, experiments are performed to derive mathematical relations for specific phenomena and to establish empirical correlations, as is the case with ignition delay. Regarding ignition delay, these experiments are vital in acquiring specific constants for various reactant mixtures. Once these constants are determined, ignition delay can be simulated and calculated using Arrhenius-type dependences. Various Arrhenius-type correlations exist; for instance, one equation utilized by Tang et al. [19] in their study of ignition delay times for different argon-diluted mixtures is presented in Equation 1.

$$\tau = A\phi^{\alpha}p^{\beta}exp\left(\frac{E_a}{RT}\right) \quad (1)$$

where τ is the ignition delay; A, α, β are correlation parameters, ϕ is the equivalence ratio, p denotes pressure, E_a is the activation energy, R is the universal gas constant, and T denotes temperature [19]. This equation already by itself tells a lot about how ignition delay responds to the thermodynamic conditions. The equation tells that ignition delay decreases exponentially with increasing temperature.

Equation 1 is slightly different compared to the generic version of the Arrhenius equation; it uses the equivalence ratio instead of the masses or moles of the oxidizer and the fuel. Equivalence ratio is a more informative parameter for defining mixture composition. Its fundamental nature comes from its ability to standardize the reactivity potential when comparing different fuels. Equivalence ratio also fundamentally dictates the thermodynamic properties of the mixture, and it is the primary variable dictating both the ignition delay and the laminar flame speed [7].

1.4.2 Laminar flame speed

Similar to ignition delay, empirical data must be collected to enable accurate simulations by validating the various chemical reaction mechanisms. Unlike in the previous section, however, the methods to empirically measure laminar flame speeds are considerably more variable. Commonly used methods include the spherically expanding flame (SEF) technique, different burner configurations (heat flux, Bunsen) and shock tubes. The necessity for diverse measurement methods stems from the flame's tendency to behave differently across different thermodynamic states. Consequently, the experimental method is selected to suit the particular state measured [16].

To illustrate, Durocher et al. [21] utilized a burner method to measure the laminar flame speeds of premixed hydrogen-air-argon stagnation flames. The flame was observed in a vessel equipped with sapphire glass windows to allow for optical access. A non-intrusive laser was employed to illuminate seeded particles, and similar to the ignition delay measurements, OH* chemiluminescence was tracked to identify the flame front. By tracking these particle velocities using two-dimensional Particle Tracking Velocimetry (PTV), it is possible to mathematically derive the laminar flame speeds [21].

After a multitude of flame speed experiments, a sufficient amount of data is collected, and a framework is established to perform calculations or simulations such as those executed utilizing Cantera. While there are many different mathematical relations for laminar flame speed, the generally used power-law form presented by Goodman et al. [16] in their study of ammonia-air laminar flame speeds under different conditions is illustrated in Equation 2.

$$S_L = S_{L,0} \left(\frac{T}{T_0}\right)^{\alpha} \left(\frac{P}{P_0}\right)^{\beta} \quad (2)$$

where S_L is the laminar flame speed, $S_{L,0}$ represents the reference flame speed, T and T_0 are the unburned gas temperature and reference temperature, respectively, P and P_0 denote the pressure and reference pressure, respectively, and α and β are the temperature and pressure empirical exponents. Determining these constants is one of the primary objectives of the mentioned experimental studies. The power-law dependence of the laminar flame speed on temperature and pressure can be clearly observed form the equation.

1.4.3 Influence of the diluent gas

In the field of combustion, the composition of the diluent gas is a critical parameter. Traditional internal combustion engines utilize ambient air as an oxidizer mixture, which is considered to consist of 21% oxygen (O_2) and 79% nitrogen (N_2) by volume. Therefore, in conventional applications, nitrogen naturally serves as the primary diluent gas [7]. Furthermore, these gases act as the primary working fluid of the cycle. While the use of ambient air is operationally highly convenient, nitrogen is not necessarily the optimal diluent gas. Novel engine concepts, such as the Argon Power Cycle, replace atmospheric nitrogen with argon (Ar) as the diluent gas. Experiments utilizing this technology have yielded promising results regarding thermal efficiency and other fundamental combustion metrics [6].

The reason why the diluent gas is so important in combustion theory stems from many different standpoints. One of them becomes highly evident when working with highly reactive and combustible fuels such as the hydrogen observed in this study. With elevated activity comes the risk of uncontrolled combustion. When working with a rich mixture, this challenge becomes even more evident. Uncontrolled combustion leads to engine knock, which in turn causes mechanical damage to the engine and its components [7]. When analyzing how the diluent affects the combustion reaction, the molecular level must be observed. The diluent gas in the fuel mixture effectively reduces the probability of the fuel and oxidizer molecules colliding and forming activated complex molecules, thus making the reaction more controlled [22].

When it is desired to compare the performance and efficiency of internal combustion engines, thermal efficiency is the key parameter. The thermodynamic basis for the Argon Power Cycle is based on an idealized Otto cycle, whose efficiency can be calculated with Equation 3 [7].

$$\eta_{Th} = 1 - \frac{1}{r_c^{\gamma-1}} \quad (3)$$

where η_{Th} is the thermal efficiency, r_c is the compression ratio, and γ is the specific heat ratio. By analyzing this equation, it can be derived that the specific heat ratio is the dominating variable when analyzing how the working fluid choice affects the thermal efficiency. Since the specific heat ratio is the dominating variable in the equation, choosing a working fluid with a higher specific heat ratio directly increases the thermal efficiency. Nitrogen (N_2) is the primary working fluid for traditional internal combustion engines. Since nitrogen is a diatomic molecule, its specific heat ratio is determined to be 1.4, but at real operating temperatures, it drops even further to 1.33. Unlike nitrogen, argon (Ar) is a monatomic molecule due to it being a noble gas. Monatomic gases inherently possess a higher specific heat ratio of approximately 1.67 [6]. This fundamental difference in molecular structure makes argon a significantly more thermodynamically efficient working fluid.

As detailed by Jin et al. [6], although the use of argon provides superior thermal efficiency, this feature introduces a notable problem in combustion. The definition of the specific heat ratio denotes that argon's higher value mathematically dictates a lower specific heat capacity; in practical terms, this means argon requires significantly less energy to raise its temperature compared to nitrogen. A lower specific heat capacity entails that the argon molecules are not able to absorb as much heat from the reaction compared to nitrogen, thus serving as a significantly less effective heat sink. This ineffectiveness leads to much higher operating temperatures compared to conventional air-breathing engines, which in turn can lead to engine knock. Conventionally, engine knock prevention is achieved by decreasing the compression ratio (r_c) or adding anti-knock agents to the fuel. Regarding Argon Power Cycle engines, knock can be mitigated by running a highly diluted mixture with an abundance of argon, thereby increasing the overall thermal mass to compensate for the lower heat capacity. Furthermore, knock

can also be controlled by injecting a low amount of water into the intake port with only a marginal effect on the efficiency [6].

Despite presenting a greater knock risk, the higher operating temperatures significantly accelerate the combustion kinetics. As demonstrated by Equations 1 and 2, an increase in temperature inherently dictates an increased laminar flame speed and a shorter ignition delay time.

2. Kinetic modeling approach

As stated before, computational modeling with Cantera inherently relies on specific assumptions and limitations. Rather than simulating the entire engine environment, the software isolates the fundamental chemical reaction kinetics. In real-world combustion engines, numerous physical phenomena make the overall process highly complex. This makes the accurate modeling using idealized computational tools not feasible. These real-world complexities include three-dimensional turbulence, heat losses to the combustion chamber walls, and complex fluid dynamics. By removing these physical disturbances, Cantera allows for a highly focused analysis of the underlying chemical behavior. These simplified simulations for the ease of computing are not in line with the values that would be from a real-world engine, but they serve as a great preliminary base for future testing and more sophisticated simulations.

2.1 Ignition delay modeling

To model ignition delay, certain simplifications were made. Ignition delay time (τ) being a scalar quantity allows for simulating it in the zeroth dimension (0D). This idealization is only possible if the reactor is assumed to be perfectly stirred and homogeneous with uniform thermodynamic properties. To assess the fuel mixtures, Cantera's adiabatic constant-pressure reactor (IdealGasConstPressureReactor) was utilized [9].

The use of this simulation model determines that the adiabatic boundary condition does not allow for any heat exchange while the gas mixture freely expands and maintains constant pressure. This is because the temperature increase is desired to be only affected by the chemical reactions of the mixture. For this study, the ignition delay time is defined as the time interval from the start of the simulation to the moment of the peak concentration of the hydroxyl (OH) radical, which serves as an indicator for the onset of ignition [6].

In the research for the best-suited kinetics library for the encountered fuels observed and conditions simulated in this study, AramcoMech 3.0 offered the best and most extensive capabilities, since the simulation is particularly accurate for hydrogen and small hydrocarbons such as methane. It is also far more extensive compared to the

older mechanism, GRI-Mech 3.0, which was frequently found in studies. The selection of this exact mechanism aimed to result in as precise results as possible with the simplified simulation models by using the mechanism with the most defined combustion mechanisms at different temperatures and pressures. AramcoMech 3.0 also captures the interactions between the fuel, oxidizer, and diluent really accurately, making the analysis of ignition delay and laminar flame speed as precise as possible [23].

The only fundamental difference between the simulation of the two different fuels was the temperature range. Ignition delay for hydrogen was simulated in temperature range of 900 – 1600 K, which was sufficient to model the ignition. For methane the starting temperature had to be increased resulting in a range of 1100 – 1600 K. Methane requires more heat to ignite, the higher starting temperature helps to simulate the ignition process within a reasonable timeframe, avoiding excessively long delay times.

The diluent and oxidizer mixture utilized is 21% oxygen and 79% argon (by mole fraction), which is chosen for its similar composition to ambient air (21% oxygen and 79% nitrogen). This makes the comparison between traditional air-breathing engines and Argon Power Cycle engines more feasible. Three different equivalence ratios were used: ϕ = 0.5 (lean), ϕ = 1 (stoichiometric), ϕ = 2 (rich), while the pressure was kept at a constant 1 atm. To get results as similar as possible compared to real-life engine applications, both constant-pressure and changing-pressure simulations were utilized. For these simulations the mixture was kept at a stoichiometric equivalence ratio (ϕ = 1), and the pressure was varied from 1 - 100 bar at selected temperatures (1000 – 1100 K for hydrogen and 1100 – 1200 K for methane). To ensure numerical accuracy, the simulation time step is managed by Cantera's solver to be several orders of magnitude smaller than the anticipated ignition delay, allowing for a precise capture of the rapid chemical induction phase.

All simulation results will be visualized by using the Matplotlib library in Python. The code used will be found in Appendices as Appendix 1.

2.2 Laminar flame speed modeling

Unlike ignition delay, the laminar flame speed (S_L) is a spatial phenomenon, thus requiring a spatial domain for accurate modeling. The phenomenon involves the propagation of a flame front through the mixture. To simulate the flame's nature, a one-dimensional (1D) simulation is utilized to account for the internal structure of the flame, including the preheat and reaction zones. For this purpose, Cantera's freely propagating adiabatic flame model is utilized [9].

The 1D simulation assumes a steady-state condition where the unburned gas mixture flows into the flame front at a velocity that matches the flame's speed. To solve the governing equations of mass, energy, and species conservation, the model incorporates molecular transport properties. In this study, a mixture-averaged transport model is employed to calculate species diffusion and thermal conductivity [9].

To maintain consistency with the zero-dimensional ignition delay calculations, the detailed AramcoMech 3.0 mechanism was utilized in the laminar flame speed calculations, despite making the computational strain more notable compared to lighter models such as GRI-Mech 3.0. To simulate the parameters as accurately as possible with the simplified modeling tools in use, the following decisions were made. The domain for the simulations was selected to be large enough that all the reactions had enough space to take place and reach completion, and the temperature gradients and concentrations had enough room to disappear at the boundaries. For the free flame solver, which solves the deep gradients within the flame front, adaptive grid refinement provided by Cantera was utilized. The maximum allowed gradient (slope) was selected as 0.07, and the maximum allowed curvature was chosen to be 0.14. As with the ignition delay simulation code, the code for the laminar flame speed calculation can be found in the appendices as Appendix 2.

3. Results

This section aims to present the simulation results and analyze them. The main goal is to analyze and compare the results of the two fuel mixtures: hydrogen/oxygen/argon and methane/oxygen/argon. The parameters analyzed will be the before-mentioned ignition delay time and laminar flame speed. Additionally, data from existing studies about the combustion characteristics of traditional air-breathing engines will be presented to make a baseline for argon comparison and evaluation.

3.1 Ignition delay

The ignition delay times were calculated for hydrogen and methane mixtures over temperature ranges of 900–1600 K and 1100–1600 K, respectively. The simulations were performed at a constant pressure of 1 atm across three different equivalence ratios (ϕ = 0.5, 1.0, 2.0). Figures 1 and 2 illustrate the ignition delay times as a function of inverse temperature for both fuels.

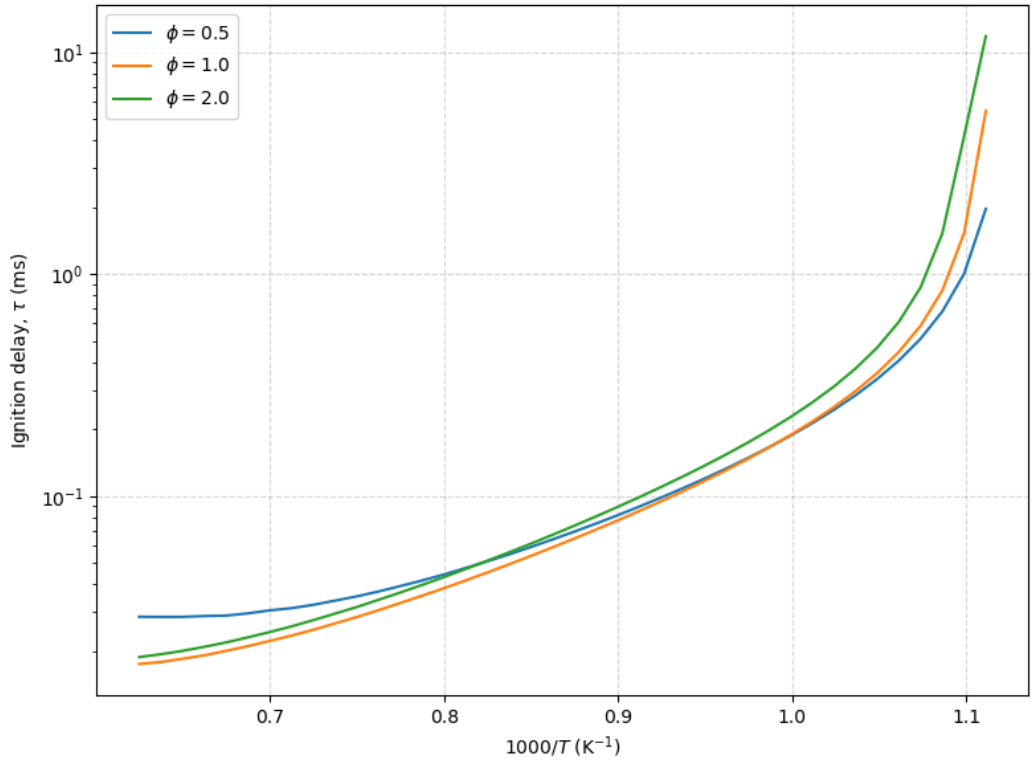

Figure 1: Computed ignition delay times of hydrogen/oxygen/argon mixture as a function of inverse temperature at a constant pressure of 1 atm, across varying equivalence ratios (ϕ = 0.5, 1.0, 2.0).

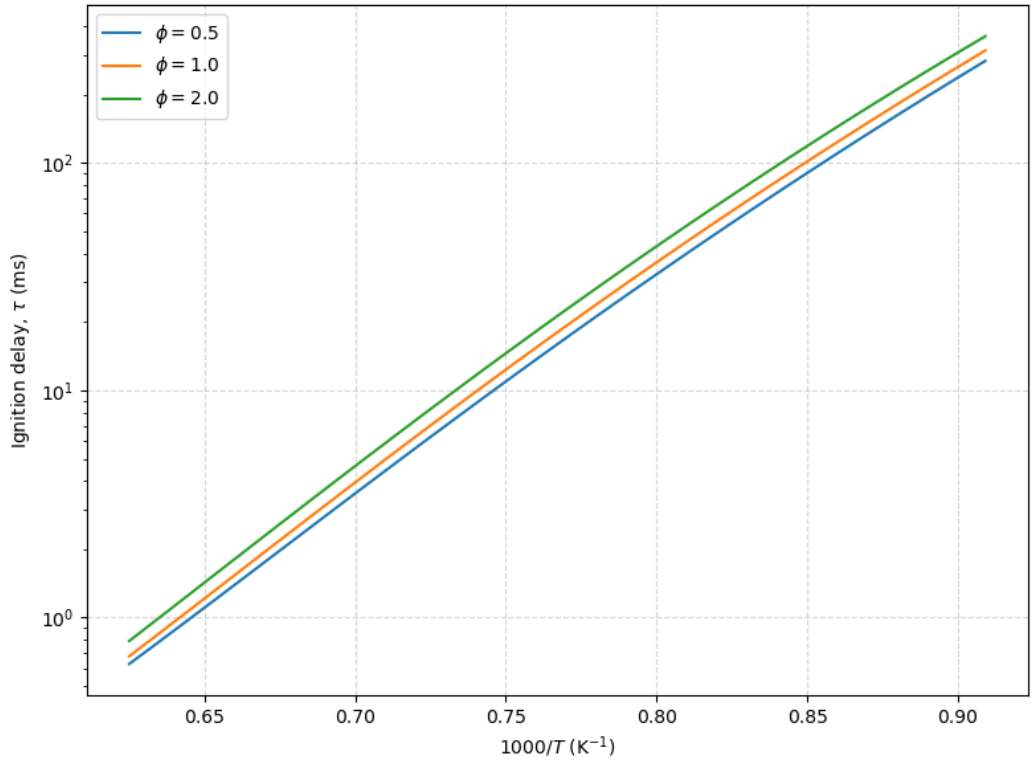

Figure 2: Computed ignition delay times of methane/oxygen/argon mixture as a function of inverse temperature at a constant pressure of 1 atm, across varying equivalence ratios (ϕ = 0.5, 1.0, 2.0).

Even though vastly different, the two fuel mixtures of hydrogen and methane exhibit the same fundamental behavior of decreased ignition delay time caused by increased temperature. This is in line, as expected, with the governing combustion theory. Some differences can still be observed; methane has linear behavior on the logarithmic scale, which indicates that the mixture has a highly Arrhenius-type relationship with the inverse temperature. The hydrogen mixture exhibits more complicated behavior, since its graph lines curve instead of being linear. This suggests that hydrogen is highly sensitive to the changes in the temperature and suffers notably more from a decrease in temperature compared to methane.

When comparing the two fuels, it is evident that they react quite differently to the changes in equivalence ratio. Methane is the less sensitive of the two. Methane has only a minor reaction to the change in equivalence ratio, and the lean mixture of ϕ = 0.5 has the shortest delay across the whole range, while the rich mixture has the longest. The relative difference between the different equivalences stays mostly the same for the whole range. As a complete opposite to the monotonic behavior of methane, the

hydrogen mixture reacts to the changes in equivalence ratio vastly differently. At the initial conditions, the stoichiometric mixture exhibits the shortest ignition delay, but at the middle of the temperature range at roughly 1000 K, the behavior changes and a crossover happens, and at the end of the temperature range, the lean mixture achieves the shortest delay time, while the rich mixture has the longest, and the stoichiometric mixture finishes between these two. This crossover indicates hydrogen's sensitivity to the changes in equivalence ratio.

With the data shown in the constant pressure diagrams, it can be concluded that hydrogen is significantly more reactive compared to methane. Hydrogen also exhibits notably shorter ignition delay times for most of the temperature range.

To learn more about the ignition behavior of methane and hydrogen mixtures, the ignition delay times were calculated as a function of pressure, with the pressure ranging from 1 to 100 bar. The simulation conditions were chosen to be stoichiometric (ϕ = 1.0) and three different temperatures of 1000 K, 1050 K, and 1100 K for hydrogen, and 1100 K, 1150 K, and 1200 K for methane, were chosen. Figures 3 and 4 show the results of these simulations.

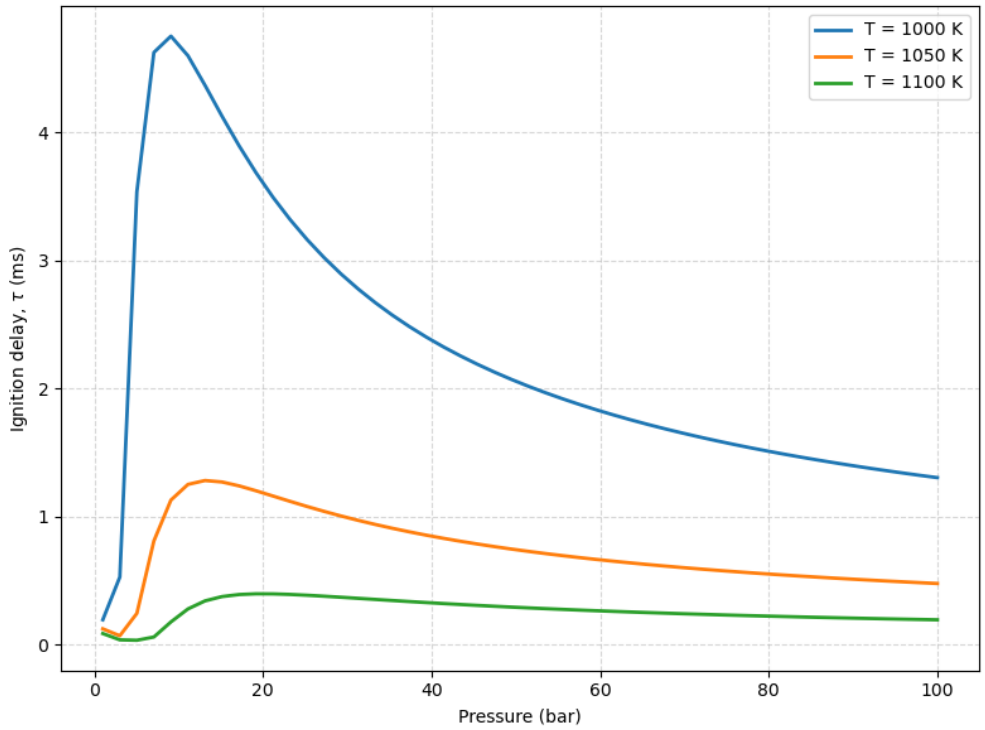

Figure 3: Computed ignition delay times of hydrogen/oxygen/argon mixture as a function of pressure at a stoichiometric equivalence ratio (ϕ=1.0), across varying temperatures of 1000 K, 1050 K and 1100 K.

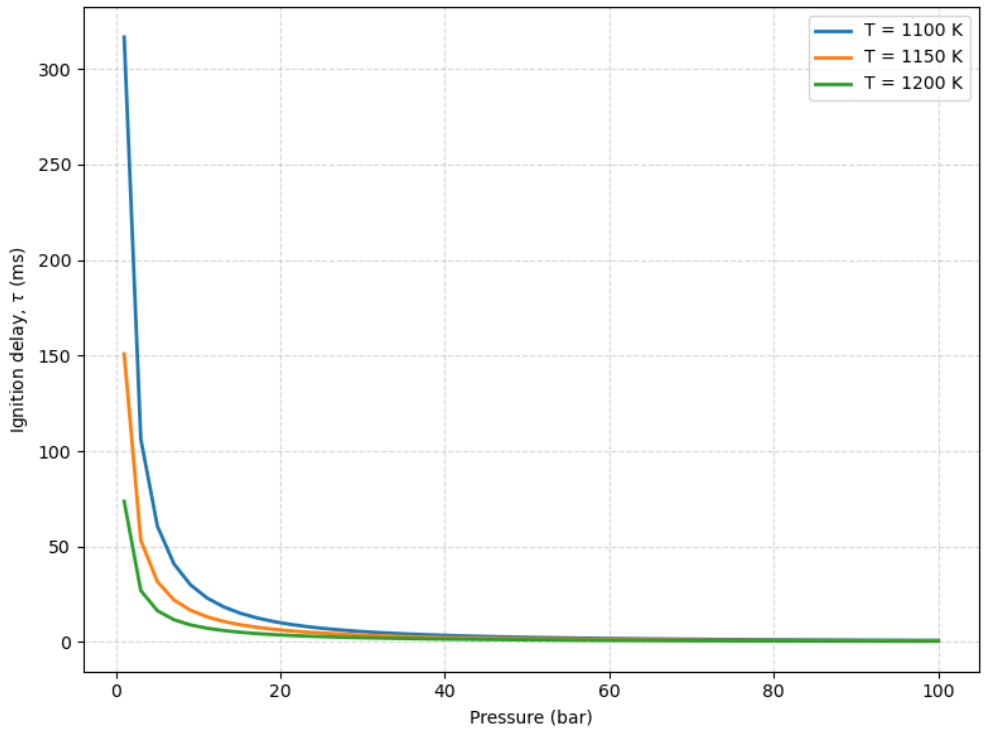

Figure 4: Computed ignition delay times of methane/oxygen/argon mixture as a function of pressure at a stoichiometric equivalence ratio (ϕ=1.0), across varying temperatures of 1100 K, 1150 K and 1200 K.

When observing Figures 3 and 4, it becomes evident that for both of the fuels, the increase in pressure shortens the ignition delay. Methane's decrease happens in a quite exponential fashion, but hydrogen exhibits more complex behavior. As the pressure starts to increase from the initial, it can be observed that the ignition delay actually starts to increase instead of decreasing. This strange behavior between 0 and 10 bars is due to one of hydrogen's features, its second explosion limit. In these zero-dimensional simulations, it shows the kinetic competition where pressure-dependent recombination reactions begin to dominate over the chain-branching *OH* radical product, which temporarily acts as a chain-terminating process [24]. After the pressure is increased beyond 10 bars, the reaction chain changes, and hydrogen's ignition delay time starts to decrease as expected.

Since both mixtures react differently to the increased pressure, methane's behavior is vastly different from hydrogen's. As the pressure rises, methane's ignition delay time sharply decreases until approximately 20 bars. After the 20 bar point, the methane mixture does not notably benefit from the elevated pressure anymore. Additionally, the effect of the initial temperature almost completely vanishes after the 20 bar point, and all the different temperature lines converge. This is highly different compared to hydrogen, where the effect of the initial temperature was visible even at highly elevated pressures. Hydrogen has quite monotone behavior at 1100 K initial temperature and continues almost unchanged through the whole pressure range, but at the 1000 K initial temperature it reacts vastly differently and keeps on decreasing for the whole pressure range.

As was established in the earlier temperature analyses, hydrogen is in most conditions more reactive than methane and thus possesses a shorter ignition delay time. It should be noted, though, that at highly elevated pressures a crossover occurs, and methane is able to reach a shorter ignition delay compared to hydrogen.

In conclusion, hydrogen is the more reactive fuel of the two. All the results are brought together in one graph in Figure 5. This figure gives a clear image of how these two fuel mixtures compare to each other. The simulation conditions are the same as those used in Figures 1 and 2.

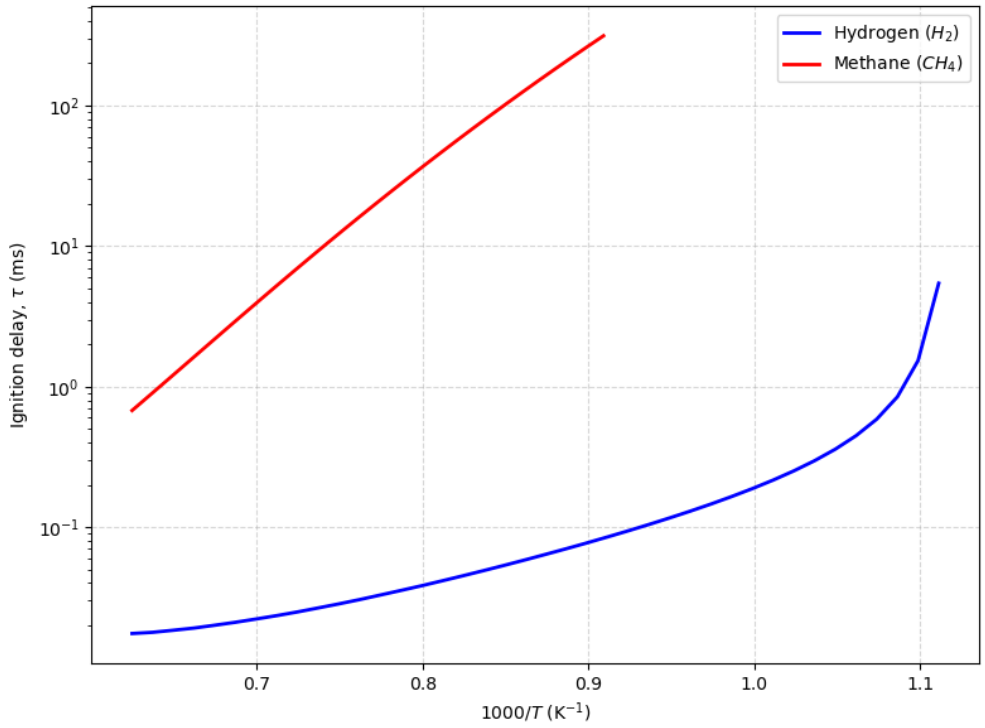

Figure 5: Comparison of ignition delay times for hydrogen and methane mixtures as a function of inverse temperature at 1 atm pressure and varying equivalence ratios (ϕ = 0.5, 1.0, 2.0).

Figure 5 provides a clear picture of the two fuels. From the figure, it can be concluded that hydrogen is the more reactive fuel. It should also be noted that hydrogen remains more reactive despite changes in the equivalence ratio.

3.2 Laminar flame speed

The laminar flame speeds (S_L) were simulated for both fuel mixtures, methane and hydrogen. The simulation aims to highlight the flame propagation characteristics of these two fuels. The simulations were performed as a function of the equivalence ratio between 0.5 and 2.0. The conditions were set to a pressure of 1 atm and initial temperatures of 300 K and 700 K. Both fuels used the same initial conditions. The results can be found in Figures 6 and 7.

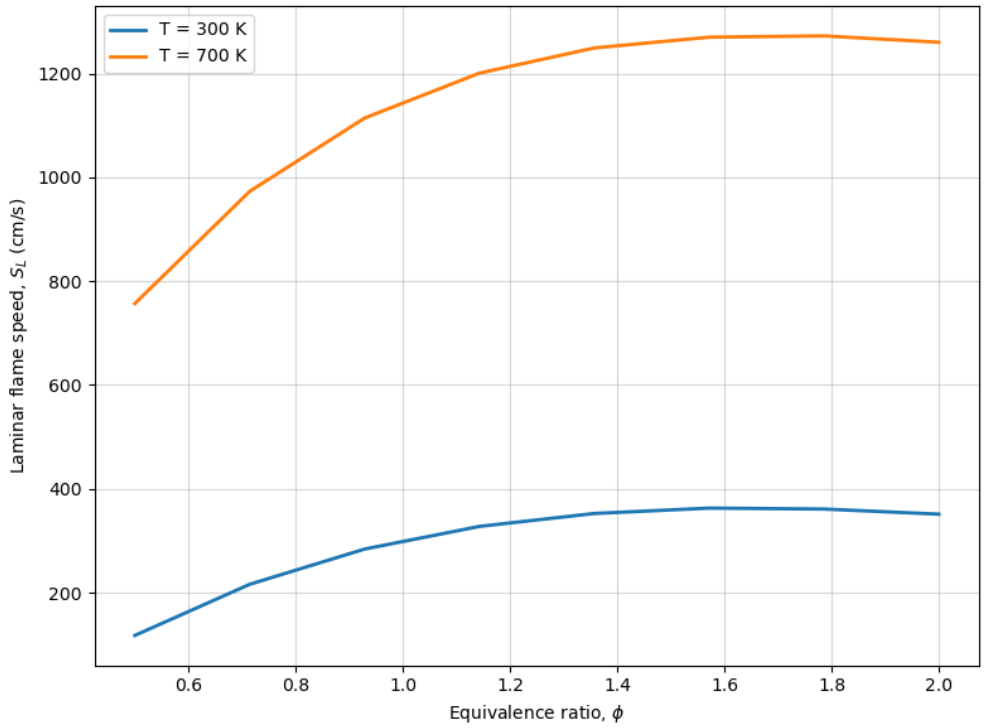

Figure 6: Computed laminar flame speeds of a hydrogen/oxygen/argon mixture as a function of equivalence ratio at a constant pressure of 1 atm, with initial temperatures set to 300 K and 700 K.

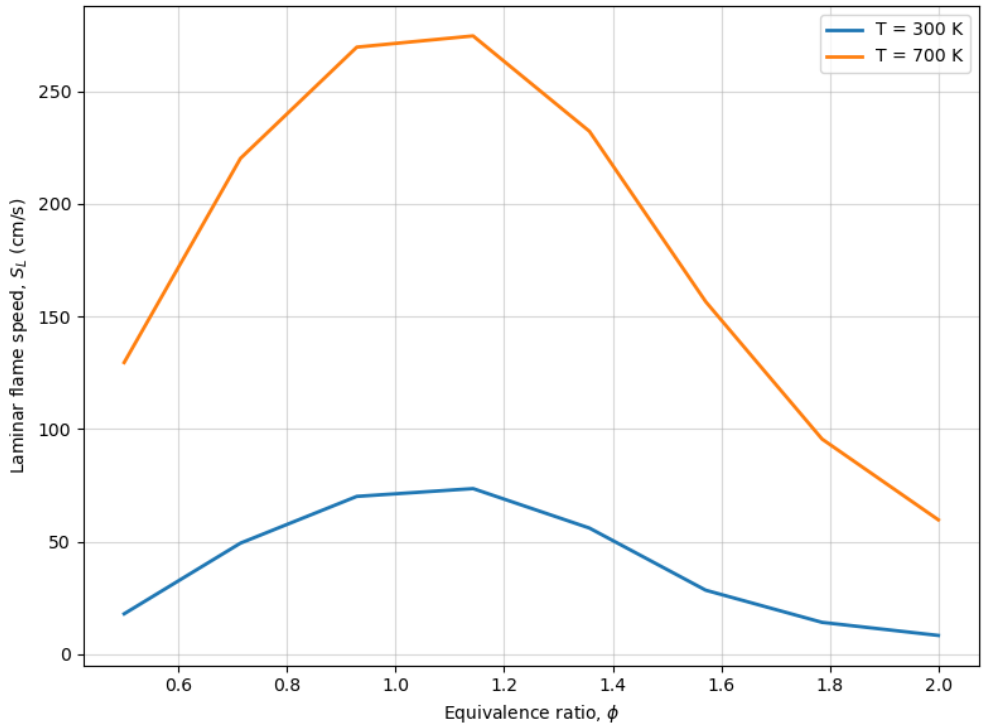

Figure 7: Computed laminar flame speeds of a methane/oxygen/argon mixture as a function of equivalence ratio at a constant pressure of 1 atm, with initial temperatures set to 300 K and 700 K.

An evaluation of the two fuels reveals completely different responses to changes in the equivalence ratio. When observing the hydrogen mixture, a clear dependency of the laminar flame speed on the equivalence ratio is evident. The flame speed reaches its maximum in the fuel-rich region, and in line with combustion theory, the increase in temperature accelerates the flame propagation speed. For methane, the behavior is different; it reaches its maximum speed near stoichiometry ($\phi \approx 1.15$), unlike hydrogen. When moving further into the fuel-rich region, the flame speed decreases rapidly. Methane, like hydrogen, indicates a positive connection between the laminar flame speed and initial temperature, meaning this holds true for both mixtures.

When comparing the two mixtures, a clear difference can be seen in their flame propagation characteristics. The hydrogen mixture achieves its maximum flame speed at approximately 1300 cm/s, while the methane mixture only reaches a speed of around 280 cm/s at its maximum. This reveals that hydrogen is 4.5 times faster than methane. Under identical thermodynamic conditions, the hydrogen mixture exhibits a substantially higher overall reactivity.

To get a more complete picture of the behavior of the fuel mixtures, the simulations were also performed as a function of temperature to evaluate the effect of pressure. Both mixtures were simulated at stoichiometric conditions ($\phi = 1.0$) and initial pressures of 1 bar and 40 bar across a varying temperature range. Figures 8 and 9 present the simulation results for both fuel mixtures.

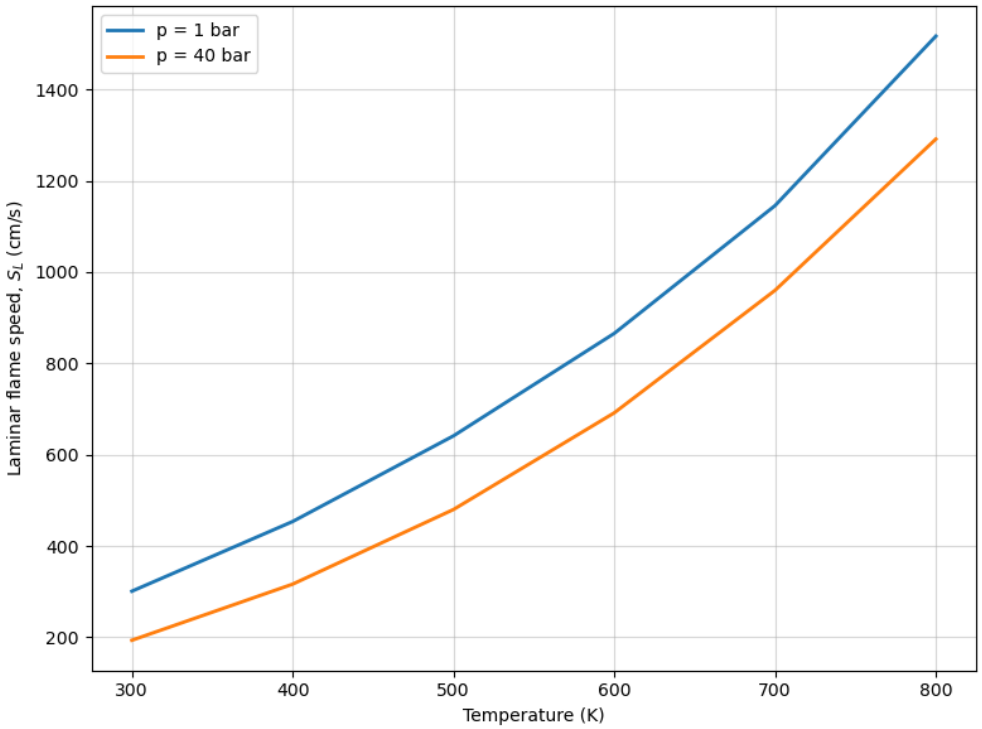

Figure 8: Computed laminar flame speeds of the hydrogen/oxygen/argon mixture as a function of temperature. The simulations were performed at a stoichiometric equivalence ratio (ϕ = 1.0) under initial pressures of 1 bar and 40 bar.

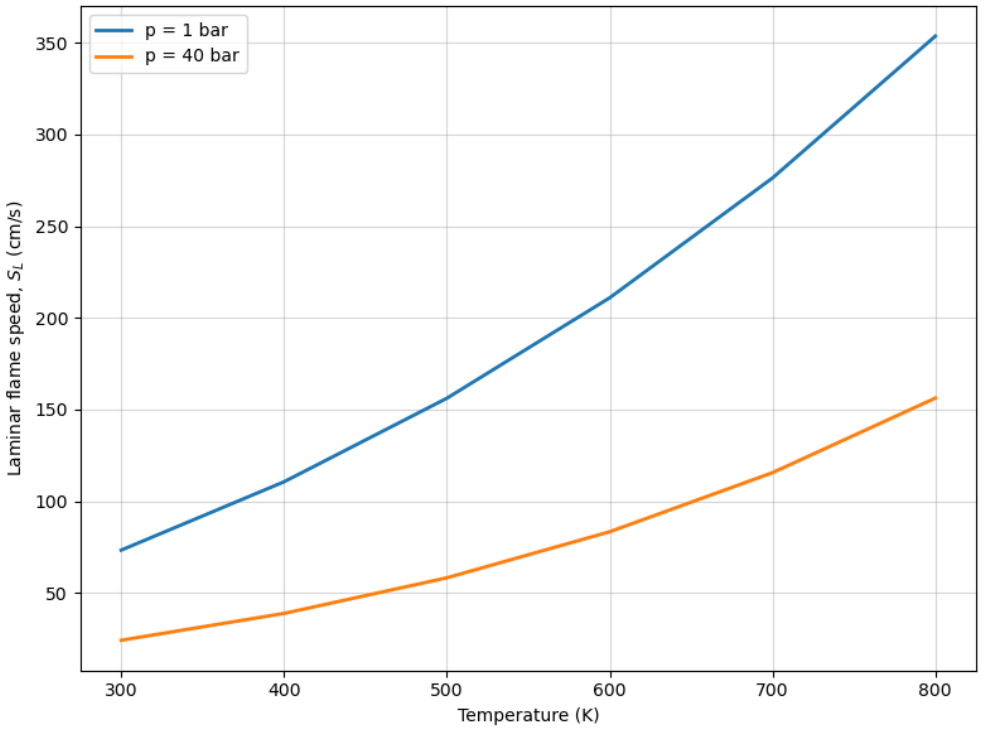

Figure 9: Computed laminar flame speeds of the methane/oxygen/argon mixture as a function of temperature. The simulations were performed at a stoichiometric equivalence ratio (ϕ = 1.0) under initial pressures of 1 bar and 40 bar.

When comparing the two graphs, a similar behavior can be seen regarding the pressure. Figures 8 and 9 illustrate that increasing the initial pressure critically affects the laminar flame speed. These findings are in line with combustion theory, and this decrease in flame speed due to increased pressure occurs because the increase in pressure also increases the gas density. Denser gas has lower thermal diffusivity, so more time is required to transfer the heat required to ignite the adjacent gas. Even though elevated pressures gave a better ignition delay time, the opposite is true for the laminar flame speed. Methane is more sensitive to pressure changes compared to hydrogen, as is visible from the figures.

The figures illustrate the vital role of the initial temperature of the unburned gas in combustion. As expected, and detailed in the theoretical section of the thesis, the increased temperature accelerates the chemical kinetics, thus leading to increased flame speeds. This behavior aligns perfectly with established combustion theory. As noted in the previous section, temperature and pressure act as the primary thermodynamic variables dominating the flame propagation characteristics.

Across all the simulated conditions—pressures and temperatures—hydrogen exhibits a significantly more reactive nature compared to methane. Hydrogen's laminar flame speed constantly exceeds methane's by approximately 4.5 times. These results show hydrogen's ideal nature in the Argon Power Cycle and demonstrate its excellent flame propagation capabilities in these conditions.

3.3 Comparison with nitrogen diluted mixtures

Since the goal of the thesis is to compare the use of argon as a working fluid against nitrogen, experimental data on the use of nitrogen was collected from the literature. The found data about the ignition delays of the nitrogen-diluted hydrogen and methane

mixtures can be found in Figures 10 and 11. The ones that present the laminar flame speed of the nitrogen-diluted mixtures can be found in Figures 12 and 13.

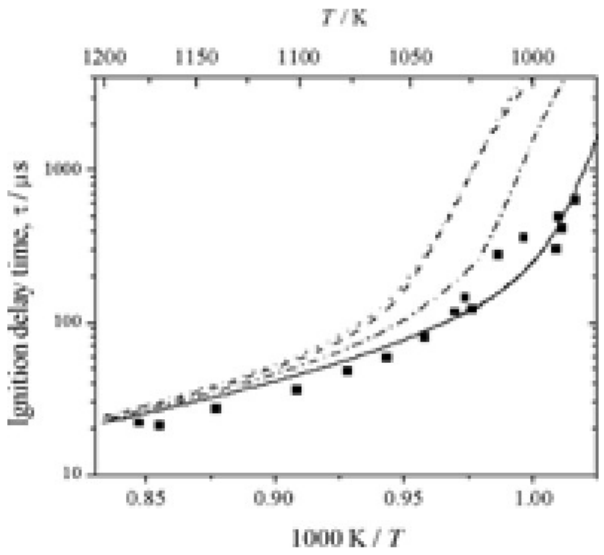

Figure 10: Ignition delay times (τ) for stoichiometric hydrogen/air mixtures at 2 atm pressure as a function of inverse temperature (1000/T). The symbols (▪) represent experimental shock tube data from [25], and the lines indicate various chemical kinetic model predictions. Adapted with permission from [26].

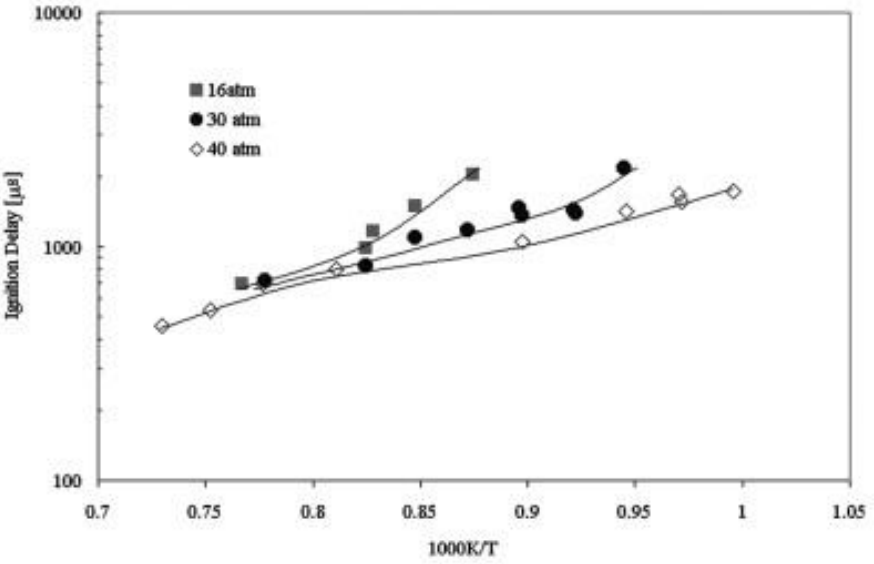

Figure 11: Experimental ignition delay times (τ) for stoichiometric methane/air mixtures at various initial pressures. The symbols represent shock tube measurements from [27]. The plot demonstrates the pressure-dependent ignition behavior in nitrogen-diluted systems. Adopted with permission from [27].

When comparing the simulated data and experimental data, a notable difference can be observed between the two dilutions. From Figures 10 and 11, it can be seen that the nitrogen-diluted values are generally longer compared to the argon-diluted ones across

the majority of the temperature range. A value of 0.25 ms can be observed for the argon-diluted hydrogen in Figure 1, and the nitrogen-diluted value in the same thermodynamic conditions of 1000 K and the same equivalence ratio is 0.5 ms. This shows that the hydrogen is approximately twice as fast in the argon mixture compared to the nitrogen mixture. This finding is in line with the theory about the effects of molar heat capacity, discussed in Chapter 1.4.3.

Methane shows a more complex behavior. Since the temperature range of the simulated methane values did not completely align with the experimental data from the literature, the values had to be interpolated. The ignition delay value from the interpolation is approximately 30 ms at 1000 K and 40 bar at stoichiometry. For the air-diluted experimental data (Figure 11), the ignition delay value for the same conditions is roughly 1.8 ms. This is likely due to the extreme dilution needed for the monatomic argon. This may lead to **a** severe enough reduction in reactions that the kinetic decrease is significantly **greater than** the benefits.

As predicted in Chapter 1.4.3, the higher specific heat ratio (γ) of argon leads to increased operating temperatures. This in turn accelerates ignition of hydrogen. However, the requirement for high dilution to mitigate knock (as also discussed in 1.4.3) explains the observed kinetic retardation in the methane mixture.

In addition to ignition delay times, the laminar flame speed (S_L) serves as a fundamental indicator of the mixture's reactivity and its ability to sustain a stable combustion process. Figures 12 and 13 present the comparison between the simulated argon-diluted flame speeds and the experimental nitrogen-diluted benchmarks for hydrogen and methane, respectively.

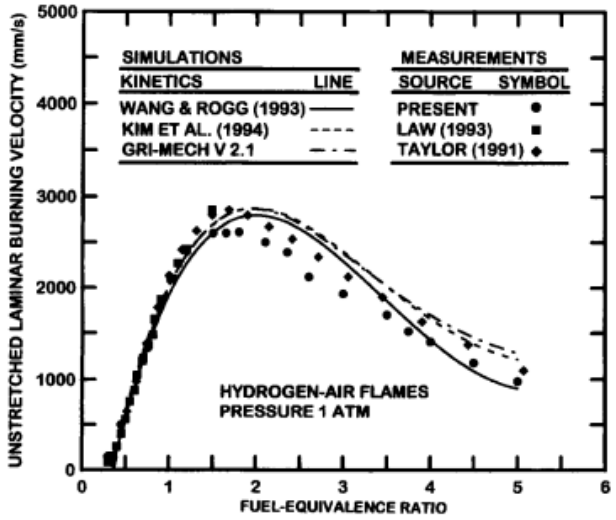

Figure 12: Comparison of experimental and simulated laminar burning velocities (S_L) for atmospheric hydrogen/air mixtures across varying equivalence ratios (ϕ). Velocity values are presented in mm/s. Adopted with permission from [28]

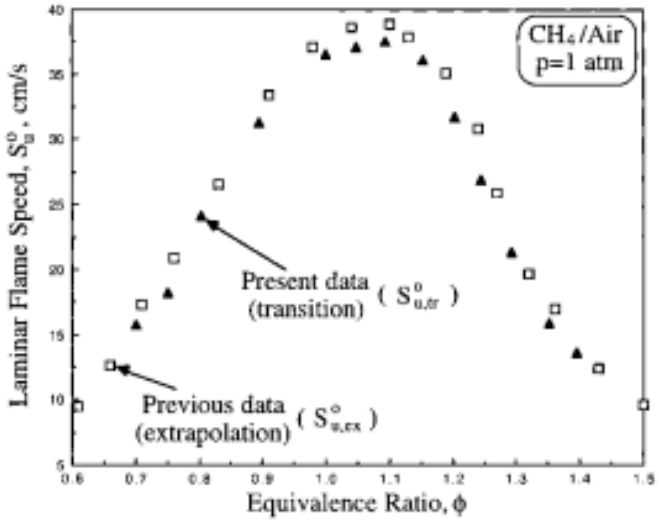

Figure 13: Comparison of experimental laminar flame speeds (S_L) for atmospheric methane/air mixtures across varying equivalence ratios (ϕ). Adopted with permission from [29].

For the hydrogen mixture (Figure 6), the computational value at 300 K, ϕ = 1.5 and pressure of 1 atm for the laminar flame speed is approximately 365 cm/s. In comparison, the experimental hydrogen-air benchmark (Figure 12) shows a speed of roughly 275 cm/s under the same parameters. This significant enhancement in the argon-diluted mixture is related to the lower heat capacity of the monatomic diluent. This yields higher adiabatic flame temperatures and accelerates the chemical kinetics.

The same trend of faster flame speeds for argon dilution can also be observed for methane. The air-diluted methane mixture peaks at 300 K and 1 atm and is approximately 40 cm/s, as demonstrated in Figure 13. This peak happens on the rich side of stoichiometry. When looking at the argon-diluted mixture (Figure 7) at the same conditions as the air-diluted one, a flame speed of approximately 75 cm/s can be observed. Even though methane's ignition delay suffered from the high dilution, the increased adiabatic flame temperatures accelerate the flame speed.

As explained in Chapter 1.4.3, the lower specific heat capacity of argon clearly benefits the kinetics of the reaction. This statement is proved by the simulation results. The lower molar heat capacity of the monatomic argon produces significantly higher adiabatic flame temperatures compared to diatomic nitrogen. Both the simulations of methane and hydrogen show a benefit from the increased temperature of the flame front caused by the use of argon. The extreme dilution causes some problems with the reactivity of methane, but both of the fuels consistently exceed the laminar flame speeds of their air-diluted counterparts.

4. Conclusions

This thesis aims to explore the Argon Power Cycle and specifically its combustion characteristics by analyzing two key parameters: laminar flame speed and ignition delay. The fuel mixtures under investigation for the cycle were hydrogen/oxygen/argon and methane/oxygen/argon. The parameters were calculated utilizing a Python code that uses the kinetics library Cantera. Additionally, the computational results were compared against those of traditional air-breathing engines to demonstrate the benefits of the Argon Power Cycle. The data of the traditional engines was collected from pre-existing literature.

When analyzing the combustion behavior of hydrogen, a trend could be observed. The use of argon as a diluent consistently increased the laminar flame speeds and lowered the ignition delay. This indicates that hydrogen substantially benefits from the use of argon as a diluent. This increased performance is due to argon's monatomic nature, which results in a lower specific heat ratio, which in turn increases the flame temperatures. The increased flame temperature accelerates the combustion reactions, thus making the hydrogen more reactive and ideal for use in the Argon Power Cycle.

While a clear benefit from the use of argon can be seen for the hydrogen, the same does not completely happen for methane. The laminar flame speed increases due to the higher adiabatic temperature caused by the use of argon compared to the air diluted one but the ignition delay grows longer in higher pressures. This is caused by the high levels of dilution to mitigate engine knock. For methane the decreased reactivity mostly outweighs the thermodynamical benefits of argon. This shows a clear trade-off when using less reactive fuels in Argon Power Cycle.

This thesis demonstrates the excellent possibilities and results that argon power cycle can achieve. The thermal benefit is clear like expected for the change from diatomic to monoatomic. With this technology a new challenge represents itself in the practical implementation side. The technology requires extremely precise and rigorous optimization of dilution levels and mixture ratios. This optimization is even more important for less reactive hydrocarbon fuels such as the methane explored in this thesis. This study highlights the benefits of the idealized argon power cycle but before

real world implementation more sophisticated modeling has to be done. Since the simulations in this thesis were done in 0D and 1D the results do not align with results achieved in real world implementations. The simulation of this behavior would require 3D computational fluid dynamics simulations. Further research should also focus on knock mitigation without compromising efficiency, like happens due to extreme dilution. Argon power cycle technology's real-life efficiency should also be confirmed by real prototype engine experiments to get as real values as possible.

References

[1] Carbon neutrality by 2050: the world's most urgent mission | Secretary-General, (2020). https://www.un.org/sg/en/content/secretary-general/articles/2020-12-11/carbon-neutrality-2050-the-worlds-most-urgent-mission (accessed April 12, 2026).

[2] A. Accardo, T. Costantino, G. Malagrinò, M. Pensato, E. Spessa, Greenhouse Gas Emissions of a Hydrogen Engine for Automotive Application through Life-Cycle Assessment, Energies 17 (2024) 2571. https://doi.org/10.3390/en17112571.

[3] A.N. Hayhurst, I.M. Vince, Nitric oxide formation from N2 in flames: The importance of "prompt" NO, Prog. Energy Combust. Sci. 6 (1980) 35–51. https://doi.org/10.1016/0360-1285(80)90014-3.

[4] S. Babamohammadi, A.R. Birss, H. Pouran, J. Pandhal, T.N. Borhani, Emission control and carbon capture from diesel generators and engines: A decade-long perspective, Carbon Capture Sci. Technol. 14 (2025) 100379. https://doi.org/10.1016/j.ccst.2025.100379.

[5] W. Chan, T. Morosuk, X. Li, H. Li, Allam cycle: Review of research and development, Energy Convers. Manag. 294 (2023) 117607. https://doi.org/10.1016/j.enconman.2023.117607.

[6] S. Jin, J. Deng, K. Xie, X. Liang, C. Wang, W. Ding, L. Li, Knock control in hydrogen-fueled argon power cycle engine with higher compression ratio by water port injection, Appl. Energy 349 (2023) 121664. https://doi.org/10.1016/j.apenergy.2023.121664.

[7] J.B. Heywood, Internal Combustion Engine Fundamentals, 2nd Edition, McGraw-Hill Education, 2018. https://www.accessengineeringlibrary.com/content/book/9781260116106 (accessed January 19, 2026).

[8] Y. Zhang, Z. Huang, L. Wei, J. Zhang, C.K. Law, Experimental and modeling study on ignition delays of lean mixtures of methane, hydrogen, oxygen, and argon at elevated pressures, Combust. Flame 159 (2012) 918–931. https://doi.org/10.1016/j.combustflame.2011.09.010.

[9] D.G. Goodwin, H.K. Moffat, I. Schoegl, R.L. Speth, B.W. Weber, Cantera: An Object-oriented Software Toolkit for Chemical Kinetics, Thermodynamics, and Transport Processes, https://www.cantera.org, 2025. https://doi.org/10.5281/zenodo.17620923.

[10] H.O. Ghareeb, H.A.A.-W. Anjal, Ignition Delay Period Prediction for Compression Ignition Engines Fueled with Ethanol/Diesel Blends, J. Eng. 30 (2024) 48–70. https://doi.org/10.31026/j.eng.2024.08.04.

[11] B. Su, M. Papp, P. Zhang, T. Turányi, Dependence of ignition delay time on its definition – A case study on methane ignition, Combust. Flame 262 (2024) 113364. https://doi.org/10.1016/j.combustflame.2024.113364.

[12] J.B. Baker, R.K. Rahman, M. Pierro, J. Higgs, J. Urso, C. Kinney, S. Vasu, Experimental Ignition Delay Time Measurements and Chemical Kinetics Modeling of Hydrogen/Ammonia/Natural Gas Fuels, J. Eng. Gas Turbines Power 145 (2022). https://doi.org/10.1115/1.4055721.

[13] É. Valkó, M. Papp, P. Zhang, T. Turányi, Identification of homogeneous chemical kinetic regimes of methane-air ignition, Proc. Combust. Inst. 39 (2023) 467–476. https://doi.org/10.1016/j.proci.2022.07.186.
[14] A. Harbi, A. Farooq, Monte-Carlo based laminar flame speed correlation for gasoline, Combust. Flame 222 (2020) 61–69. https://doi.org/10.1016/j.combustflame.2020.08.023.
[15] A.A. Konnov, A. Mohammad, V.R. Kishore, N.I. Kim, C. Prathap, S. Kumar, A comprehensive review of measurements and data analysis of laminar burning velocities for various fuel+air mixtures, Prog. Energy Combust. Sci. 68 (2018) 197–267. https://doi.org/10.1016/j.pecs.2018.05.003.
[16] J. Goodman, A. Dhankhar, A. Date, P. Lappas, Ammonia–air laminar flame speeds from ambient to IC engine conditions: A review, Fuel 383 (2025) 133769. https://doi.org/10.1016/j.fuel.2024.133769.
[17] T. Aittokoski, K. Miettinen, Cost effective simulation-based multiobjective optimization in the performance of an internal combustion engine, Eng. Optim. 40 (2008) 593–612. https://doi.org/10.1080/03052150801914429.
[18] E. Hu, L. Pan, Z. Gao, X. Lu, X. Meng, Z. Huang, Shock tube study on ignition delay of hydrogen and evaluation of various kinetic models, Int. J. Hydrog. Energy 41 (2016) 13261–13280. https://doi.org/10.1016/j.ijhydene.2016.05.118.
[19] C. Tang, X. Man, L. Wei, L. Pan, Z. Huang, Further study on the ignition delay times of propane–hydrogen–oxygen–argon mixtures: Effect of equivalence ratio, Combust. Flame 160 (2013) 2283–2290. https://doi.org/10.1016/j.combustflame.2013.05.012.
[20] X. Man, C. Tang, L. Wei, L. Pan, Z. Huang, Measurements and kinetic study on ignition delay times of propane/hydrogen in argon diluted oxygen, Int. J. Hydrog. Energy 38 (2013) 2523–2530. https://doi.org/10.1016/j.ijhydene.2012.12.020.
[21] A. Durocher, M. Meulemans, G. Bourque, J.M. Bergthorson, Measurements of the laminar flame speed of premixed, hydrogen-air-argon stagnation flames, Appl. Energy Combust. Sci. 7 (2021) 100028. https://doi.org/10.1016/j.jaecs.2021.100028.
[22] J. Zhao, L. Zhou, K. Li, X. Zhang, J. Pan, R. Chen, H. Wei, Effect of diluent gases on end-gas autoignition and combustion modes in a confined space, Combust. Flame 222 (2020) 48–60. https://doi.org/10.1016/j.combustflame.2020.08.042.
[23] J. Xue, S. Xi, F. Wang, An extensive study on skeletal mechanism reduction for the oxidation of C0–C4 fuels, Combust. Flame 214 (2020) 184–198. https://doi.org/10.1016/j.combustflame.2019.12.035.
[24] J. Liu, W. Liang, C.K. Law, Theory of explosion limits of hydrogen/oxygen mixtures, Combust. Flame 277 (2025) 114186. https://doi.org/10.1016/j.combustflame.2025.114186.
[25] M.W. Slack, Rate coefficient for H + O2 + M = HO2 + M evaluated from shock tube measurements of induction times, Combust. Flame 28 (1977) 241–249. https://doi.org/10.1016/0010-2180(77)90031-1.
[26] M. Ó Conaire, H.J. Curran, J.M. Simmie, W.J. Pitz, C.K. Westbrook, A comprehensive modeling study of hydrogen oxidation, Int. J. Chem. Kinet. 36 (2004) 603–622. https://doi.org/10.1002/kin.20036.

[27] J. Huang, P.G. Hill, W.K. Bushe, S.R. Munshi, Shock-tube study of methane ignition under engine-relevant conditions: experiments and modeling, Combust. Flame 136 (2004) 25–42. https://doi.org/10.1016/j.combustflame.2003.09.002.
[28] K.T. Aung, M.I. Hassan, G.M. Faeth, Flame stretch interactions of laminar premixed hydrogen/air flames at normal temperature and pressure, Combust. Flame 109 (1997) 1–24. https://doi.org/10.1016/S0010-2180(96)00151-4.
[29] C.M. Vagelopoulos, F.N. Egolfopoulos, Direct experimental determination of laminar flame speeds, Symp. Int. Combust. 27 (1998) 513–519. https://doi.org/10.1016/S0082-0784(98)80441-4.

Appendices

Appendix 1

Appendix 1 contains the Python code used to simulate the ignition delay results discussed in Section 3.1. The code utilizes Cantera to model the ignition delay in a zero-dimensional (0D) reactor for both fuel mixtures.

```
import cantera as ct
import numpy as np
import matplotlib.pyplot as plt

gas = ct.Solution('AramcoMech3.0.yaml')
eqv_ratio_values = [0.5, 1.0, 2.0]

inv_T_H2 = np.linspace(1000/1600, 1000/900, 40)
T_H2 = 1000 / inv_T_H2
inv_T_CH4 = np.linspace(1000/1600, 1000/1100, 30)
T_CH4 = 1000 / inv_T_CH4

pressure_bar = np.linspace(1, 100, 50)
pressure_pa = pressure_bar * 100000

T_fixed_H2 = [1000, 1050, 1100]
T_fixed_CH4 = [1100, 1150, 1200]


def calculate_idt_T(fuel, temperatures, eqv_ratios, max_time):
    fuel_results = {eqv_ratio: [] for eqv_ratio in eqv_ratios}

    for eqv_ratio in eqv_ratios:
        for T in temperatures:
            gas.TPX = T, ct.one_atm, 'O2:0.21, AR:0.79'
            gas.set_equivalence_ratio(eqv_ratio, fuel,
'O2:0.21, AR:0.79')

            r = ct.IdealGasConstPressureReactor(gas,
clone=False)
            sim = ct.ReactorNet([r])

            t_list, oh_list = [], []
            t = 0.0

            while t < max_time:
                t = sim.step()
                t_list.append(t)
                oh_list.append(gas.X[gas.species_index('OH')])
                if r.T > T + 500:
```

```
                    break

            tau_ms = t_list[np.argmax(oh_list)] * 1000
            fuel_results[eqv_ratio].append(tau_ms)

    return fuel_results

def calculate_idt_P(fuel, temperatures, max_time):
    results = {T: [] for T in temperatures}

    for T in temperatures:
        for P in pressure_pa:
            gas.TPX = T, P, 'O2:0.21, AR:0.79'
            gas.set_equivalence_ratio(1.0, fuel, 'O2:0.21,
AR:0.79')

            r = ct.IdealGasConstPressureReactor(gas,
clone=False)
            sim = ct.ReactorNet([r])

            t_list, oh_list = [], []
            t = 0.0

            while t < max_time:
                t = sim.step()
                t_list.append(t)
                oh_list.append(gas.X[gas.species_index('OH')])
                if r.T > T + 500:
                    break

            if len(oh_list) > 0 and r.T > T + 100:
                tau_ms = t_list[np.argmax(oh_list)] * 1000
            else:
                tau_ms = max_time * 1000
            results[T].append(tau_ms)

    return results

results_T_H2 = calculate_idt_T('H2', T_H2, eqv_ratio_values,
0.1)
results_T_CH4 = calculate_idt_T('CH4', T_CH4,
eqv_ratio_values, 2.0)

results_P_H2 = calculate_idt_P('H2', T_fixed_H2, 0.1)
results_P_CH4 = calculate_idt_P('CH4', T_fixed_CH4, 2.0)


plt.figure(figsize=(8, 6))
for phi in eqv_ratio_values:
    plt.plot(1000/T_H2, results_T_H2[phi], label=fr'$\phi =
{phi}$')
```

```
plt.yscale('log')
plt.xlabel('$1000/T$ (K$^{-1}$)')
plt.ylabel(fr'Ignition delay, $\tau$ (ms)')
plt.legend()
plt.grid(True, which='major', ls='--', alpha=0.5)
plt.tight_layout()


plt.figure(figsize=(8, 6))
for phi in eqv_ratio_values:
    plt.plot(1000/T_CH4, results_T_CH4[phi], label=fr'$\phi =
{phi}$')
plt.yscale('log')
plt.xlabel('$1000/T$ (K$^{-1}$)')
plt.ylabel(fr'Ignition delay, $\tau$ (ms)')
plt.legend()
plt.grid(True, which='major', ls='--', alpha=0.5)
plt.tight_layout()


plt.figure(figsize=(8, 6))
plt.plot(1000/T_H2, results_T_H2[1.0], 'b-', linewidth=2,
label='Hydrogen ($H_2$)')
plt.plot(1000/T_CH4, results_T_CH4[1.0], 'r-', linewidth=2,
label='Methane ($CH_4$)')
plt.yscale('log')
plt.xlabel('$1000/T$ (K$^{-1}$)')
plt.ylabel(fr'Ignition delay, $\tau$ (ms)')
plt.legend()
plt.grid(True, which='major', ls='--', alpha=0.5)
plt.tight_layout()


plt.figure(figsize=(8, 6))
for T in T_fixed_H2:
    plt.plot(pressure_bar, results_P_H2[T], linewidth=2,
label=f'T = {T} K')
plt.xlabel('Pressure (bar)')
plt.ylabel(fr'Ignition delay, $\tau$ (ms)')
plt.legend()
plt.grid(True, which='major', ls='--', alpha=0.5)
plt.tight_layout()


plt.figure(figsize=(8, 6))
for T in T_fixed_CH4:
    plt.plot(pressure_bar, results_P_CH4[T], linewidth=2,
label=f'T = {T} K')
plt.xlabel('Pressure (bar)')
plt.ylabel(fr'Ignition delay, $\tau$ (ms)')
plt.legend()
```

```
plt.grid(True, which='major', ls='--', alpha=0.5)
plt.tight_layout()

plt.show()
```

Appendix 2

Appendix 2 contains the Python code used to simulate the laminar flame speed results discussed in Section 3.2. The code utilizes Cantera to model the freely propagating flames for both fuel mixtures.

```
import cantera as ct
import numpy as np
import matplotlib.pyplot as plt

gas = ct.Solution('AramcoMech3.0.yaml')
width = 0.03

eqv_ratios_sweep = np.linspace(0.5, 2, 8)
T_sweep_eqv = [300, 700]
pressure = ct.one_atm

T_sweep_T = np.linspace(300, 800, 6)
P_sweep = [ct.one_atm, 40 * 100000]
eqv_ratio_stoich = 1.0

def calculate_LFS_eqv (fuel, temperatures, eqv_ratios,
pressure):
    results = {T: [] for T in temperatures}

    for T in temperatures:
        for eqv_ratio in eqv_ratios:

            gas.TPX = T, pressure, 'O2:0.21, AR:0.79'
            gas.set_equivalence_ratio(eqv_ratio, fuel,
'O2:0.21, AR:0.79')

            try:
                f = ct.FreeFlame(gas, width=width)
                f.set_refine_criteria(ratio=3, slope=0.07,
curve=0.14)
                f.solve(loglevel=1, auto=True)

                Sl_cm_s = f.velocity[0] * 100
                results[T].append(Sl_cm_s)

            except Exception as e:
                results[T].append(np.nan)
```

```
    return results


def calculate_LFS_T(fuel, eqv_ratio, temperatures, pressures):
    results = {P: [] for P in pressures}

    for P in pressures:
        P_bar = P / 100000

        for T in temperatures:
            gas.TPX = T, P, 'O2:0.21, AR:0.79'
            gas.set_equivalence_ratio(eqv_ratio, fuel,
'O2:0.21, AR:0.79')

            try:
                f = ct.FreeFlame(gas, width=width)
                f.set_refine_criteria(ratio=3, slope=0.07,
curve=0.14)
                f.solve(loglevel=1, auto=True)

                Sl_cm_s = f.velocity[0] * 100
                results[P].append(Sl_cm_s)

            except Exception as e:
                results[P].append(np.nan)

    return results

results_eqv_H2 = calculate_LFS_eqv('H2', T_sweep_eqv,
eqv_ratios_sweep, pressure)
results_T_H2 = calculate_LFS_T('H2', eqv_ratio_stoich,
T_sweep_T, P_sweep)
results_eqv_CH4 = calculate_LFS_eqv('CH4', T_sweep_eqv,
eqv_ratios_sweep, pressure)
results_T_CH4 = calculate_LFS_T('CH4', eqv_ratio_stoich,
T_sweep_T, P_sweep)


plt.figure(figsize=(8, 6))
for T in T_sweep_eqv:
    plt.plot(eqv_ratios_sweep, results_eqv_H2[T], '-',
linewidth=2, label=f'T = {T} K')
plt.xlabel(fr'Equivalence ratio, $\phi$')
plt.ylabel(fr'Laminar flame speed, $S_L$ (cm/s)')
plt.legend()
plt.grid(True, which='major', ls='-', alpha=0.5)
plt.tight_layout()


plt.figure(figsize=(8, 6))
for P in P_sweep:
```

```
    P_bar = P / 100000
    plt.plot(T_sweep_T, results_T_H2[P], '-', linewidth=2,
label=f'p = {P_bar:.0f} bar')
plt.xlabel('Temperature (K)')
plt.ylabel(fr'Laminar flame speed, $S_L$ (cm/s)')
plt.legend()
plt.grid(True, which='major', ls='-', alpha=0.5)
plt.tight_layout()

plt.figure(figsize=(8, 6))
for T in T_sweep_eqv:
    plt.plot(eqv_ratios_sweep, results_eqv_CH4[T], '-',
linewidth=2, label=f'T = {T} K')
plt.xlabel(fr'Equivalence ratio, $\phi$')
plt.ylabel(fr'Laminar flame speed, $S_L$ (cm/s)')
plt.legend()
plt.grid(True, which='major', ls='-', alpha=0.5)
plt.tight_layout()

plt.figure(figsize=(8, 6))
for P in P_sweep:
    P_bar = P / 100000
    plt.plot(T_sweep_T, results_T_CH4[P], '-', linewidth=2,
label=f'p = {P_bar:.0f} bar')
plt.xlabel('Temperature (K)')
plt.ylabel(fr'Laminar flame speed, $S_L$ (cm/s)')
plt.legend()
plt.grid(True, which='major', ls='-', alpha=0.5)
plt.tight_layout()

plt.show()
```